Self-pulsation in an InGaN laser - theory and experiment -

Self-Pulsation in an InGaN Laser—Theory and Experiment

V. Z. Tronciu, Minoru Yamada, *Member, IEEE*, Tomoki Ohno, Shigetoshi Ito, Toshiyuki Kawakami, and Mototaka Taneya

***Abstract*—Room-temparature operation of self-pulsating InGaN lasers was obtained at a wavelength of 395 nm. The laser structure consists of a multiquantum-well InGaN active layer and a p-type InGaN single-quantum-well saturable absorber. The frequency range of the self-pulsation was from 1.6 to 2.9 GHz. The experimental results were well explained with our theoretical analysis. We found that features of the saturable absorber strongly affect the self-pulsation. Influence of device and material parameters on the laser dynamics was also investigated.**

***Index Terms*—Room temperature, saturable absorber, self-pulsation, violet InGaN laser.**

I. Introduction

During recent years, violet InGaN lasers have received considerable attention for the application to high-density optical disk storage and optical data processing. Much progress in the development of violet-blue lasers has been made since the first operation of the laser was reported by Nakamura *et al.* [1], [2]. Meanwhile, several groups have reported the CW operation at room temperature using different fabrications methods [3]–[7]. Recently, the violet laser diode (LD) performance has been improved and the lifetime has been extended to over 15 000 h. Already the 400-nm CW LDs are available commercially. Nevertheless, little has been reported on self-pulsating voilet LDs since the earlier investigation by Nakamura [8]. The phenomenon of self-pulsation (SP) is considered to be the most important for reduction of the feedback noise [9]–[11].

In this paper, we focus on generation of SP in a multiquantum-well (MQW) InGaN laser with an additional p-type InGaN saturable absorber (SA). The peak of the emission spectrum was observed around 395 nm. In the fabrication process, the SA layer was grown in parallel to the active region. However, the additional growth of an SA layer complicates the fabrication and tends to increase the threshold current. The purpose of this study is to describe the self-pulsating characteristics of an InGaN MQW laser with an SA, which can generate self-pulsations at room temperature. In Section II, we present the laser structure, model, and equations. In Section III, numerically simulated results and experimental data of a self-pulsating InGaN laser are shown. Good agreement between measured and calculated characteristics of InGaN laser self-pulsations are demonstrated. Also in Section III, we study how the laser and material parameters influence the laser dynamics. Finally, the conclusions are given in Section IV.

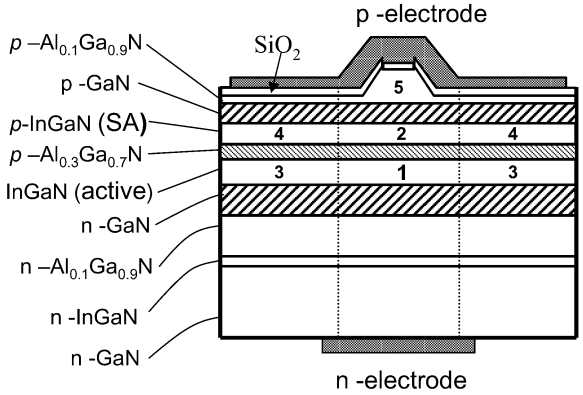

Fig. 1. Schematic view of the InGaN laser.

II. Laser Structure, Model, and Equations

An analytical model of self-pulsating laser is shown in Fig. 1. The theoretical analysis is based on structure of actually fabricated laser samples [12], [13]. The model consists of the InGaN active layer and a p-type InGaN layer as an SA. Parameters used in the calculations are shown in Table I. The active layer is composed of six QWs (well $In_{0.07}Ga_{0.93}N$, barrier $In_{0.02}Ga_{0.98}N$), while the SA is a single QW. The thickness of the SA ranges from 1 to 3 nm. Most of numerical calculations in this paper have been carried out for lasers with a 3-nm thickness of the SA. Such a thin layer is preferable to prevent increase of the threshold current. On the other hand, too thin an SA layer reduces the operating range of self-pulsation. The influence of thickness of the SA on the dynamics will be discussed in more detail in Section III. The p-type $Al_{0.3}Ga_{0.7}N$ layer is set as an evaporation-preventing layer between the active region and the SA. More details on the device fabrication are given in [13]. Since the active and SA layers are separated by an evaporation-preventing layer, we assume different carrier lifetimes in the active region and in the SA. Our treatment differs from previous ones [9], [10], where the SA and the active regions are

Manuscript received February 20, 2003; revised August 26, 2003. The work of V. Z. Tronciu was supported by the Japan Society for the Promotion of Science (JSPS) and previously from a Royal Society NATO grant and the Alexander von Humboldt Foundation.

V. Z. Tronciu is with the Department of Electrical and Electronic Engineering, Faculty of Engineering, Kanazawa University, Kanazawa, 920-8667, Japan and also with the Department of Physics, Technical University of Moldova, Chisinau, MD2004 Republic of Moldova (e-mail: tronciu@ec.t.kanazawa-u.ac.jp).

M. Yamada is with the Department of Electrical and Electronic Engineering, Faculty of Engineering, Kanazawa University, Kanazawa, 920-8667, Japan (e-mail: myamada@t.kanazawa-u.ac.jp).

T. Ohno, S. Ito, T. Kawakami, and M. Taneya are with the Device Technology Research Laboratories, Sharp Corporation, Nara 632-8567, Japan.

Digital Object Identifier 10.1109/JQE.2003.819541

TABLE I
PARAMETERS USED IN NUMERICAL CALCULATIONS

Symbol	Definition	Value & units
Active regions		
a_{active}	Differential gain coefficient	1.85×10^{-12} m^{3}s^{-1}
N_g(active)	Transparent carrier density	1.4×10^{25}m^{-3}
τ_s	Carrier life time	2.0 ns
d_{active}	Thickness	18nm
W_{active}	Width	2.0μm
Saturable absorber		
a_{SA}	Differential gain coefficient	13.0×10^{-12}m^{3}s^{-1}
N_g(SA)	Transparent carrier density	2.6×10^{25}m^{-3}
τ_s	Carrier life time	0.1 ns
d_{SA}	Thickness	3 nm
W_{SA}	Width	2.0μm
Other parameters		
λ	Wavelength	395nm
R_f	Reflectivity at the front facet	0.2
R_b	Reflectivity at the back facet	0.9
I_{leak}	Leak current	0.35 I_{th}
κ	Losses	15 cm^{-1}

made of the same material and have the same value for the carrier lifetime. Lasers with different cavity lengths 350, 500, and 650 μm have been investigated.

The theoretical model used in this paper originates from Yamada [14], [15]. The rate equations of laser operation are

$$\frac{dS}{dt}=\left[\frac{\sum_i a_i\xi_i(N_i-N_{gi})}{V_i}-BS-G_{th}\right]S+\frac{M\sum_i a_i\xi_i N_i}{V_i} \tag{1}$$

$$\frac{dN_i}{dt}=-\frac{a_i\xi_i}{V_i}(N_i-N_{gi})S-\frac{N_i}{\tau_{si}}+\sum_{j\neq i}\left(\frac{N_j}{T_{ij}}-\frac{N_i}{T_{ji}}+\frac{I_{ji}-I_{ij}}{e}\right) \tag{2}$$

where S is the photon number, N_i is the injected carrier number in the $i$the region, a_i is the differential gain coefficient, ξ_i is the field confinement factor, N_{gi} is the transparent carrier number, τ_{si} is the carrier lifetime, and T_{ij} is an equivalent lifetime giving the carrier diffusion from j to i region. I_{ji} gives the carrier injection from the j to the i region. M is the equivalent total number of the longitudinal modes [16]. V_i is the volume expressed by $V_i = W_i d_i L$, where L is the laser length and d_i and W_i are thickness and width of the region, respectively. B is the gain saturation coefficient

$$B=\frac{9\pi c\tau_{in}^2}{2\varepsilon_0 n_r^2\hbar\lambda_0}\frac{|R_{cv}|^2(N-N_{g1})a_1\xi_1^2}{V_1^2} \tag{3}$$

where n_r is the refractive index, λ_0 is the central wavelength of the laser, R_{cv} is the dipole moment, and $\tau_{\rm in}$ is the intraband relaxation time. The threshold gain level $G_{\rm th}$ is given by

$$G_{\rm th}=\frac{c}{n_r}\left(\kappa+\frac{1}{2L}\ln\frac{1}{R_fR_b}\right) \tag{4}$$

where R_f and R_b are the reflectivities at the front and the back facets, respectively, and κ is the material loss coefficient.

The laser regions are separated in central and outer parts as shown in Fig. 1. In the numerical calculations, we take into account four dynamical regions which are the central active region 1, the saturable absorber 2, and the outer regions 3 and 4. The other regions have been taken into account for calculations of the effective refractive index, near field patterns and confinement factors. The region 5 is the cap layer, which is electrically connected to the external current source. The total injected current I at the electrode consists of the original driving current I_0 flowing into the active region, current component I_d that is induced by diffusion between the central and outer regions of the SA, and the leak current I_l as

$$I = I_0 + I_d + I_l. \tag{5}$$

The original driving current flowing from electrode 5 into active region 1 is written as $I_0 = I_{51}$. The diffusion current is given by $I_d = e(N_2/T_{24} - N_4/T_{42})$, where N_2 and N_4 are the carrier numbers in the central and outer regions of the SA, respectively. The leak current is assumed to be proportional with a fix ratio to the total current as $I_l = 0.35I$. For more details on the calculation procedure of the carrier injection terms I_{ij}, see [15].

The field distribution in the transverse cross section is analyzed by the effective refractive index method [14], [17], where differences of the refractive indices and the gain loss are taken into account. We evaluated the refractive index as a function of the wavelength and alloy composition. The results show that the field is concentrated mainly in the central region. In the calculations, we take into account variation of the field distribution due to variation of the carrier density during the self-pulsation. The effective volumes of outer regions 3 and 4 and the field confinement factors ξ_i of all regions are not constant and have been evaluated during the pulsations.

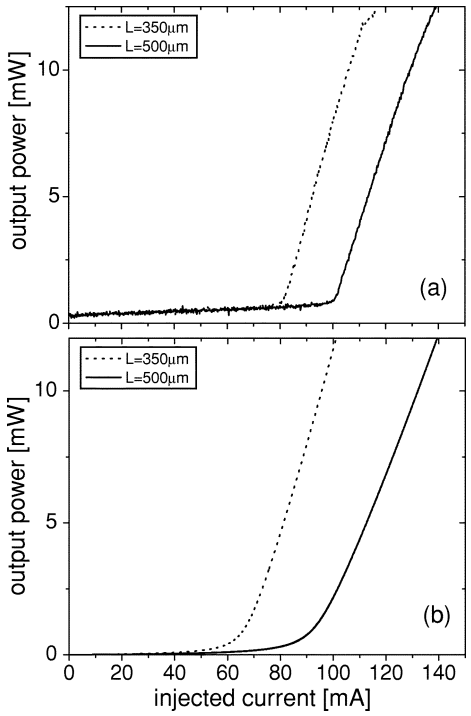

Fig. 2. Light output power versus injected current characteristic for different cavity laser length. (a) Experimentally measured data. (b) Theoretically calculated results basing on numerical parameters listed in Table I.

III. RESULTS AND DISCUSSIONS

Fig. 2(a) shows the experimentally measured L–I (light output power versus injection current) characteristics of the self-pulsating InGaN lasers for different cavity lengths. These

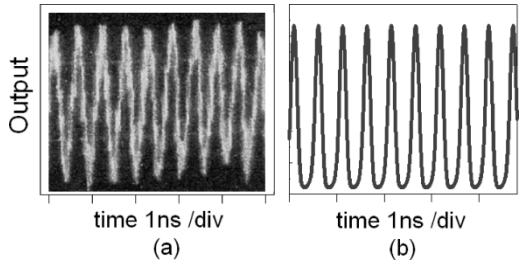

Fig. 3. (a) Measured and (b) calculated pulse traces of a 650-μm cavity length laser and 185-mA supplied injected current. The other parameters have been chosen as in Table I.

characteristics show the threshold currents of 80 and 100 mA for 350- and 500-μm cavity laser lengths, respectively. The experimental investigations of self-pulsations were performed under 1.6-μs pulsed currents at room temperature. We used pulsed current to avoid heating at the high operation currents. The threshold currents in lasers without SA are approximately half of those of lasers with the SA. Since this paper concentrates on self-pulsations, the CW operation properties of a laser without an SA are not mentioned here.

We have examined the dynamics of the InGaN laser using (1)–(5) and parameters given in Table I. Fig. 2(b) shows theoretical calculations of the light output power versus injected current for the same cavity lengths as in Fig. 2(a). The output power is calculated using

$$P_{\text{out}} = \frac{(1-R_f)\pi c^2 \hbar \bar{S}}{n_r \lambda_0 L} \frac{\ln\left(\frac{1}{R_f R_b}\right)}{(1+\sqrt{R_f R_b})(1-\sqrt{R_f R_b})} \quad (6)$$

where $\bar{S}$ is the time-averaged value of the photon number. This figure is the first indication of the agreement between experimental results and numerical simulations.

Both experiments and theoretical calculations demonstrate the presence of self-pulsation. In case of the laser with a 650-μm cavity length, the self-pulsation can be achieved experimentally for injected current in a range from 163 to 220 mA with a frequency range from 1.6 to 2.25 GHz. A typical experimental oscilloscope trace is shown in Fig. 3(a). The self-pulsation is almost stable during 1.6-μs pulse duration of the injection current. Fig. 3(b) shows the calculated pulse trace for the laser with the 650-μm cavity length and an injected current of 185 mA. The frequency of the pulsation shown in Fig. 3(b) coincides with that of Fig. 3(a) and is approximately 2 GHz.

We next examine the laser dynamics in terms of bifurcation diagrams. A typical calculation of bifurcation for the periodic solution is shown in Fig. 4(a). This figure shows the dependence of the peak of the photon number on the injected current. When we increase the injected current, the CW operation is observed (thin solid line) just after the threshold current. Then the laser begins to produce pulsations through a Hopf bifurcation marked by a circle in Fig. 4(a). This characteristic differs from that of other self-pulsating lasers reported in [14], [18], and [19], where the self-pulsation starts from the threshold current. In the previous work, the carrier lifetime in the SA region is assumed to be same as that in the active region. However, the carrier lifetime of the SA region in this paper is set to be 0.1 ns which

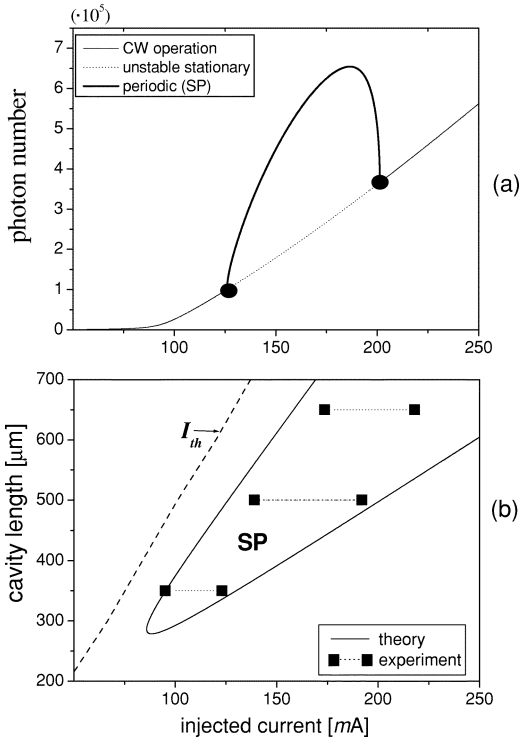

Fig. 4. (a) A typical bifurcation diagram for a 500-μm cavity length. Thin solid line indicates CW operation, while the dotted line represents the branch of unstable solutions. Thick solid line shows the peak of stable periodic solution (limit cycle). The circles indicate the Hopf bifurcation points. (b) Self-pulsation region in the plane of the laser cavity length versus the injected current. Dashed line indicates the threshold current. Experimentally obtained ranges of the self-pulsation are indicated with dotted lines terminated by blok squares.

is much smaller than that of 2.0 ns in the active region. The peak of the pulsation amplitude reaches the maximum and the self-pulsation disappears at the upper Hopf point. Both Hopf points are supercritical. We should note here that the short carrier lifetime in the SA region is believed to be caused by the piezoelectric and tunnelling effects, in the single-quantum-well structure [13], [20], [21].

The region of self-pulsation is illustrated in the plot of laser cavity length versus injected current, as shown in Fig. 4(b). The solid line indicates the position of Hopf bifurcation. The Hopf line gives the boundary between the CW and self-pulsating operations. This line has been calculated using (1)–(5) with InGaN laser parameters (see Table I). The dashed line shows the threshold current. Experimentally obtained ranges of the self-pulsation are indicated with dotted lines terminated by block squares. We note that, in the case of the laser with a 650-μm cavity laser length, we stopped the current injection at 220 mA due to the upper limit of the pulse current generator. The experiment and the theory agree very well, as found from this figure. The following features can be concluded.

1) Self-pulsation region enlarges for longer cavity length.
2) A shorter cavity length laser gives a lower threshold current, meanwhile this leads to the disappearance of the self-pulsation region.
3) The cavity length range from 350 to 650 μm is considered to be more appropriate for the InGaN laser to generate self-pulsations.

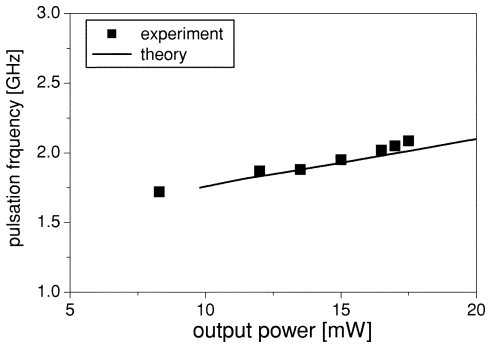

Fig. 5. Comparison between calculated (line) and measured (square) dependence of pulsing frequency on output power for a 650-μm cavity length laser diode.

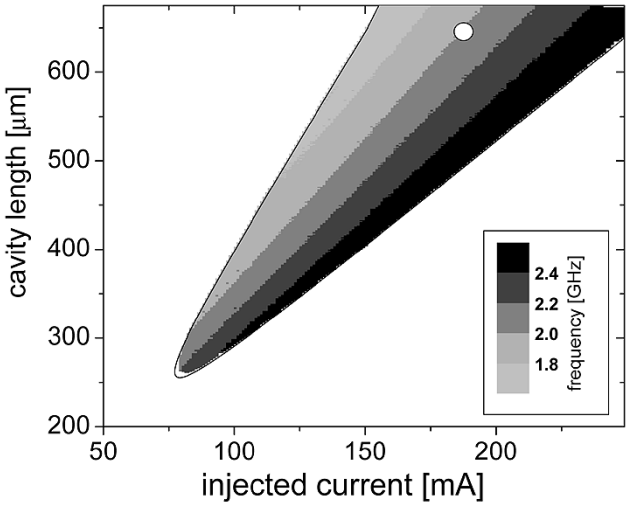

Fig. 6. Variation of frequency of self-pulsations in the plane of the cavity length versus the injected current. Darken regions are the self-pulsation regions. The white region corresponds to the CW or nonlasing operations. The white circle is the operating point given in Fig. 3(b).

In the next step, the self-pulsation frequency was analyzed. Fig. 5 shows an example of dependence of the pulsation frequency on output power for a laser with a 650-μm cavity length. The solid line corresponds to the numerical simulation. This figure demonstrates once again that the theoretical results are in close agreement with the experimental data which are indicated by squares. The self-pulsation frequency increases monotonically with increasing output power. In order to estimate the self-pulsation frequency, the numerical simulations were carried out in the plane of the cavity length versus the injected current. The results are plotted in Fig. 6, where the darkened regions are the self-pulsating regions and the white region corresponds to the CW operation or nonlasing operation. The white circle is the operation point given in Fig. 3(b). It can be seen how the self-pulsation frequency changes in the plane of these two parameters. For a fixed injected current, the pulsation frequency becomes the higher for the shorter cavity length.

In addition, we examined the influence of device and material parameters on the laser dynamics. Fig. 7(a) and (b) show calculated curves for regions of the self-pulsation in the plane of parameters of the active region and the SA. The laser cavity length is 500 μm. First we discuss the possible variations of the

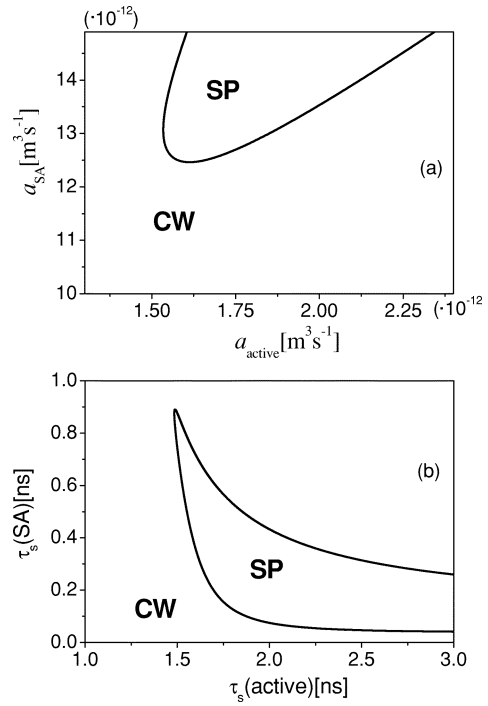

Fig. 7. The region of self-pulsations in the plane of the active region versus the SA parameters. (a) Variation of differential gain coefficient. (b) Carrier lifetime variation. The laser cavity length is 500 μm.

differential gain coefficients in the active region and in the SA. The solid line in Fig. 7(a) gives the boundary between the CW and the self-pulsation region in the plane of these two parameters. Here, the CW region indicates the nonlasing or CW operations. In the case of $a_{\rm active} < 1.5 \times 10^{-12}$ m$^3 \cdot$ s^{-1}, the laser shows the CW or nonlasing operations. This criterion is valid when the other parameters are fixed as in Table I. However, the large differential gain in the active region is not a sufficient condition to obtain the self-pulsation. The appearance of self-pulsation also depends on the differential gain in the SA. For calculations in Figs. 2–6, these two parameters are fixed to be $a_{\rm active} = 1.85 \times 10^{-12}$ m$^3 \cdot$s^{-1} and $a_{\rm SA} = 13.0 \times 10^{-12}$ m$^3 \cdot$s^{-1} as listed in Table I.

Next, we investigate the influence of the carrier lifetime on the performance of the self-pulsation. As it has been reported in [1] and [2], the carrier lifetime in an InGaN MQW LD was estimated in a range from 1.8 to 3 ns. In our calculations, we fixed the carrier lifetime in the active region to be 2 ns. However, the carrier lifetime in the SA seemS to be shorter than that in the active region. Recently it has been found that the carrier lifetimes drastically decrease from 2.5 to 2 ps with increasing reverse bias in a single-quantum-well structure made of InGaN–GaN [20]. This decrease was attributed to piezoelectric and tunneling effects. Dependence of the carrier lifetime on the well width in an InGaN single quantum well was also reported in [21]. The carrier recombination was found to be dominated by nonradiative processes. By increasing the well width from 1 to 6 nm, the carrier lifetime was found to increase from 180 to 340 ps. We demonstrated experimentally that self-pulsating operation occurred in the InGaN laser with a very short carrier lifetime in the SA but was not observed in the case of long carrier lifetime in the SA [13]. The value used in most calculations for

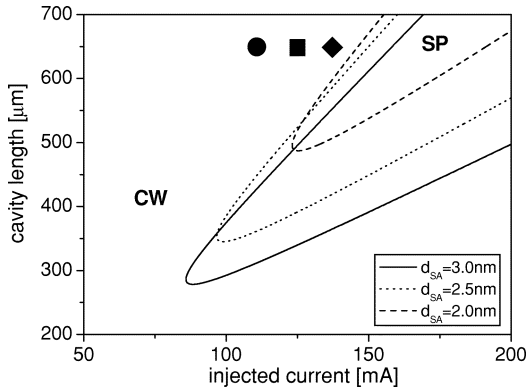

Fig. 8. Influence of thickness of the SA on the self-pulsation region. The symbols show the threshold current for lasers with a 650-μm length and different thickness of SA. Circle, squares and rhombus correspond to $d_{SA} = 2, 2.5,$ and 3 nm, respectively.

the carrier lifetime in the SA has been fixed to be 0.1 ns in this paper. Here, as shown in Fig. 7(b), we examined the effect of the carrier lifetime in the active region and in the SA on self-pulsation by keeping all other parameters equal to the values listed in Table I. The result shows the following features: when the carrier life time in the active region is smaller than 1.5 ns, only the CW operation can be observed. For large value of the carrier lifetime in the active region, a low value of the carrier lifetime in the SA is required to obtain the self-pulsating operation. This corresponds to an increase of absorbtion level in the saturable absorber.

As mentioned above, characteristics of the self-pulsation strongly depend on features of the SA. Let us consider here the influence of the saturable absorber thickness on the laser evolution. The thickness of the SA affects the field confinement factor ξ_2, the carrier lifetime, and the carrier overflow. Fig. 8 shows the self-pulsation region in the plane of the cavity length versus the injected current for different values of thickness of the SA. The lines in Fig. 8 represent the boundaries between the CW and the self-pulsation region. The variation of the thickness from 1 to 3 nm is considered to be appropriate for our fabricated lasers. For the thinner SA, the self-pulsation region becomes the smaller. This character can be explained as a consequence of decrease of the SA thickness, which induces a small value of the confinement factor ξ_2. Nevertheless, the decrease in the SA thickness leads to lower threshold currents. This result is confirmed in Fig. 8 by the symbols, which indicate theoretically calculated threshold currents for lasers with a 650-μm cavity length. The circle, square, and rhombus correspond to $d_{\mathrm{SA}} = 2, 2.5,$ and 3 nm, respectively. Thus, we have shown that a thiner SA implies lower threshold current and a reduced self-pulsation region.

IV. Conclusion

In this paper, we have presented both theoretical simulation and experimental data for self-pulsation of InGaN lasers with an SA. The lasing wavelength was 395 nm. Operation of the laser has been modeled using the Yamada model adapted to the specific case of the InGaN laser with SA. Self-pulsation in the range from 1.6 to 2.9 GHz has been confirmed. Good agreement was obtained between measurements and theoretical simulations. It was found that the thickness of the SA as well as the carrier lifetime in the SA play major roles in the laser dynamics. Although the self-pulsation in InGaN lasers involves complex phenomena, we believe that our treatment can be regarded as a good basis for further research to improve self-pulsation characteristics of InGaN lasers.

Acknowledgment

One of the authors, V. Z. Tronciu, expresses his gratitude for the hospitality of the group of Prof. M. Yamada at Kanazawa University.

References

[1] S. Nakamura, M. Senoh, S. Nagahama, N. Iwasa, T. Yamada, T. Matsushita, Y. Sugimoto, and H. Kiyoku, "Optical gain and carrier lifetime of InGaN multi-quantum well structure laser diodes," *Appl. Phys.Lett.*, vol. 69, pp. 1568–1570, 1996.

[2] S. Nakamura, S. Pearton, and G. Fasol, *The Blue LaserDiode*, 2nd ed. Berlin, Germany: Springer, 2000.

[3] T. Takeuchi, H. Takeuchi, S. Sota, H. Sakai, H. Amano, and I. Akasaki, "Optical properties of strained AlGaN and GaInN on GaN," *Jpn. J. Appl. Phys.*, vol. 36, pp. L177–179, 1997.

[4] T. Kobaiasi, T. Kobayashi, F. Nakamura, K. Naganuma, T. Tojyo, H. Nakajima, T. Asatsuma, H. Kawai, and M. Ikeda, "Room-temperature continuous-wave operation of GaInN/GaN multiquantum well laser diode," *Electron. Lett.*, vol. 34, pp. 1494–1495, 1998.

[5] A. Kuramata, S. Kubota, R. Soejima, K. Domen, K. Horino, and T. Tanahashi, "Room-temperature continuous wave operation of InGaN laser diodes with vertical conducting structure on SiC substrate," *Jpn. J. Appl. Phys.*, vol. 37, pp. L1373–L1375, 1998.

[6] M. Kuramoto, C. Sasaoka, Y. Hisanaga, Y. Hisanaga, A. Kimura, A. A. Yamaguchi, H. Sunakawa, N. Kuroda, M. Nido, A. Usui, and M. Mizuta, "Room-temperature continuous-wave operation of InGaN multi-quantum -well laser diodes groun on an n-GaN substrate with a backside n contact," *Jpn. J. Appl. Phys.*, vol. 38, pp. L184–L186, 1999.

[7] M. Kneissl, D. P. Bour, C. G. Van de Walle, L. T. Romano, J. E. Northrup, R. M. Wood, M. Teepe, and N. M. Johnson, "Room-temperature continuous-wave operation of InGaN multiple-quantum-well laser diodes with an asymmetric waveguide structure," *Appl. Phys. Lett.*, vol. 75, 581, 1999.

[8] S. Nakamura, M. Senon, S. Nagahama, N. Iwasa, T. Yamada, T. Matsushita, H. Kryoku, Y. Sugimoto, T. Kozaki, H. Umemoto, M. Sano, and K. Chocho, "InGaN/GaN/AlGaN – based laser diodes with modulation -doped strained-layer superlattices," *Jpn. J. Appl. Phys.*, vol. 36, pp. L1568–L1571, 1997.

[9] M. Yamada, "Theoretical analysis of noise-reduction effect in semiconductor laser with help of self-sustained pulsation phenomena," *J. Appl. Phys.*, vol. 79, pp. 61–71, 1996.

[10] S. Matsui, H. Takiguchi, H. Hayashi, S. Yamamoto, S. Yano, and T. Hijikata, "Suppression of feedback-induced noise in short-cavity V-channeled substrate inner stripe lasers with self-oscillation," *Appl. Phys. Lett.*, vol. 43, pp. 219–221, 1983.

[11] S. Yamashita, A. Ohishi, T. Kajimura, M. Inoune, and Y. Fukui, "Low-noise AlGaAs lasers grown by organo-metallic vapor phase epitaxy," *IEEE J. Quantum Electron.*, vol. 25, pp. 1483–1388, 1989.

[12] T. Yuasa, Y. Ueta, Y. Tsuda, A. Ogawa, M. Taneya, and K. Takao, "Effect of slight misorientation of sapphire substrate on metalorganic chemical vapor deposition growth of GaN," *Jpn. J. Appl. Phys.*, vol. 38, 1999.

[13] T. Ohno, S. Ito, T. Kawakami, and M. Taneya, "Self-pulsation in InGaN laser diodes with saturable absorber layers," *Appl. Phys. Lett.*, vol. 83, p. 1098, 2003.

[14] M. Yamada, "A theoretical analysis of self-sustained pulsation phenomena in narrow-stripe semiconductor lasers," *IEEE J. Quantum Electron.*, vol. 29, pp. 1330–1336, May 1993.

[15] ——, "A theoretical analysis of quantum noise in semiconductor laser operating with self-sustained pulsations," *IEICE Trans. Electron.*, vol. E81-C, pp. 290–298, 1998.

[16] ——, "Variation of intensity noise and frequency noise with spontaneous emission factor in semiconductor laser," *IEEE J. Quantum Electron.*, vol. 30, pp. 1511–1519, 1994.
[17] ——, "Transverse and longitudinal mode control in semiconductor injection laser," *IEEE J. Quantum Electron.*, vol. QE-19, pp. 1365–1380, 1983.
[18] J. L. A. Dubbeldam and B. Krauskopf, "Self-pulsations of lasers with saturable absorber: Dynamics and bifurcations," *Opt. Commun.*, vol. 159, pp. 325–338, 1999.
[19] C. R. Mirasso, G. H. M. van Tartwijk, E. Hernandez-Garcia, D. Lenstra, S. Lynch, P. Landais, P. Phelan, J. O'Gorman, M. S. Miguel, and W. Elsaer, "Self-pulsating semiconductor lasers: Theory and experiment," *IEEE J. Quantum Electron.*, vol. 35, pp. 764–770, 1999.
[20] Y. D. Jho, J. S. Yahng, E. Oh, and D. S. Kim, "Measurement of piezoelectric field and tunneling times in strongly biased InGaN/GaN quantum wells," *Appl. Phys. Lett.*, vol. 79, pp. 1130–1132, 2001.
[21] C.-K. Sun and T.-L. Chiu, "Time resolved photoluminescence studies of InGaN/GaN single-quantum-wells at room temperature," *Appl. Phys. Lett.*, vol. 71, pp. 425–427, 1997.

V. Z. Tronciu received the first degree in physics from the State University of Moldova in 1990 and the Ph.D. degree in physical and mathematical sciences from Institute of Applied Physics, Academy of Science of Moldova, in 1995.

He is a Lecturer in the Department of Physics, Technical University of Moldova. Currently he is working as a Japan Society for the Promotion of Science (JSPS) Post-Doctoral Fellow in the Department of Electrical and Electronic Engineering, Kanazawa University, Kanazawa, Japan. Before that, he held a Royal Society/NATO Postdoctoral Fellowship, Durham, U.K. From September 1998 to August 1999, he worked in Berlin as an Alexander von Humboldt Foundation Post-Doctoral Fellow with the Photonics Group at the Institute of Physics, Humboldt University. During his research career he has worked on a number of topics, including optical bistability, switching, self-pulsation, excitability, and chaos in various optical devices. In the last five years he has concentrated his attention on the phenomena of self-pulsation and excitability in semiconductor lasers.

Minoru Yamada (M'82) was born in Yamanashi, Japan, on January 26, 1949. He received the B.S. degree in electrical engineering from Kanazawa University, Kanazawa, Japan, in 1971 and the M.S. and Ph.D. degrees in electronics engineering from the Tokyo Institute of Technology, Tokyo, Japan, in 1973 and 1976, respectively.

He joined Kanazawa University in 1976, where he is presently a Professor. From 1982 to 1983, he was a Visiting Scientist at Bell Laboratories, Holmdel, NJ. He is currently doing research work on semiconductor injection lasers, semiconductor optical switches, and unidirectional optical amplifiers.

Dr. Yamada received the Yonezawa Memorial Prize in 1975, the Paper Award in 1976, and the Achievement Award in 1978 from the Institute of Electronics and Communication Engineers of Japan.

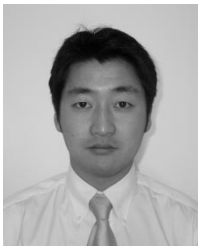

Tomoki Ohno was bom in Tokyo, Japan, on February 6, 1973. He received the B.E. and M.E. degrees in engineering from the University of Tokyo, Tokyo, Japan, in 1997 and 1999, respectively.

He joined Advanced Technology Research Laboratories, Sharp Corporation, Nara, Japan, in 1999, where he has been engaged in research and development on violet laser diodes.

Shigetoshi Ito was born in Mie, Japan, on September 24, 1966. He received the B.S. and M.S. degrees in electronics engineering from Nagoya University, Aichi, Japan, in 1989 and 1991, respectively. In 1991 he joined Advanced Technology Research Laboratories, Sharp Corporation, Nara, Japan, where he has been engaged in research and development on semiconductor laser devices.

Mr. Ito is a member of the Japan Society of Applied Physics.

Toshiyuki Kawakami received the B.S. and M.S. degrees in electronics engineering from Kyoto University, Kyoto, Japan, in 1995 and 1997, respectively.

In 2000 he joined Advanced Technology Research Laboratories, Sharp Corporation, Nara, Japan, where he has been engaged in research and development on semiconductor laser devices.

Mr. Kawakami is a member of the Japan Society of Applied Physics.

Mototaka Taneya received the B.E. and M.E. degrees in engineering from Kyoto University, Kyoto, Japan, in 1981 and 1983, respectively.

He joined Central Research Laboratories, Sharp Corporation, Nara, Japan, in 1983 and he was involved in laser diode arrays and self-pulsation-type semiconductor lasers. He was on loan to the Optoelectronics Technology Research Corporation (OTRC) from 1987 to 1989, where he worked on *in situ* lithography for quantum wire and dots of compound semiconductors. He returned to Advanced Technology Research Laboratories, Sharp Corporation, in 1990. He is now the Division Deputy General Manager of the Laboratories and has been responsible for R&D on nitride laser diodes.

Mr. Taneya is a member of the Japanese Society of Applied Physics.